Molecular simulations for adsorption and separation of natural gas in IRMOF-1 and Cu-BTC metal-organic frameworks

ARTICLE *in* PHYSICAL CHEMISTRY CHEMICAL PHYSICS · JANUARY 2009

Impact Factor: 4.49 · DOI: 10.1039/b807470d · Source: PubMed

4 AUTHORS:

Ana Martin-Calvo
Universidad Pablo de Olavide
18 PUBLICATIONS **224** CITATIONS
SEE PROFILE

E. García-Pérez
Delft University of Technology
29 PUBLICATIONS **693** CITATIONS
SEE PROFILE

J. M. Castillo
Universidad Pablo de Olavide
21 PUBLICATIONS **430** CITATIONS
SEE PROFILE

Sofia Calero
Universidad Pablo de Olavide
164 PUBLICATIONS **3,050** CITATIONS
SEE PROFILE

Molecular simulations for adsorption and separation of natural gas in IRMOF-1 and Cu-BTC metal-organic frameworks†

Ana Martín-Calvo, Elena García-Pérez, Juan Manuel Castillo and Sofia Calero*

Received 2nd May 2008, Accepted 15th July 2008
First published as an Advance Article on the web 16th October 2008
DOI: 10.1039/b807470d

We use Monte Carlo simulations to study the adsorption and separation of the natural gas components in IRMOF-1 and Cu-BTC metal–organic frameworks. We computed the adsorption isotherms of pure components, binary, and five-component mixtures analyzing the siting of the molecules in the structure for the different loadings. The bulk compositions studied for the mixtures were 50 : 50 and 90 : 10 for CH_4–CO_2, 90 : 10 for N_2–CO_2, and 95 : 2.0 : 1.5 : 1.0 : 0.5 for the CH_4–C_2H_6–N_2–CO_2–C_3H_8 mixture. We choose this composition because it is similar to an average sample of natural gas. Our simulations show that CO_2 is preferentially adsorbed over propane, ethane, methane and N_2 in the complete pressure range under study. Longer alkanes are favored over shorter alkanes and the lowest adsorption corresponds to N_2. Though IRMOF-1 has a significantly higher adsorption capacity than Cu-BTC, the adsorption selectivity of CO_2 over CH_4 and N_2 is found to be higher in the latter, proving that the separation efficiency is largely affected by the shape, the atomic composition and the type of linkers of the structure.

I. Introduction

Methane (CH_4) is one of the cleanest carbon fuels due to its low carbonaceous and particle emissions after combustion. It is also attractive for its low emissions of greenhouse gases per kW generated in industrial and energy production applications. Natural gas is composed of around 95% methane, traces of heavier gaseous hydrocarbons such as ethane (C_2H_6) and propane (C_3H_8), and other light gasses such as CO_2 and N_2. To obtain a cheap and clean fuel from natural gas it is important to purify it since the presence of CO_2 reduces the combustion power efficiency and contributes to greenhouse gas emissions.[1,2]

Metal–organic frameworks (MOFs) appear to be promising materials for storage, separation, and purification of natural gas mixtures by adsorption. They are a new class of porous materials consisting of metal-oxide clusters and organic linkers[3–9] that can form pores and cavities of a desired shape and size by selecting linkers of specific length and metals of suitable coordination.[7,9–20] Experimental and simulation studies based on the adsorption and separation of natural gas and its components in MOFs are still scarce, and most of them are focused on the adsorption isotherms of CO_2, methane, N_2, and on CO_2–CH_4 binary mixtures.[21–31]

The adsorption and separation processes of CO_2, methane, and ethane have been analyzed using molecular simulations by Wang *et al.*[21] in Cu-BTC, by Babarao *et al.*,[22] Keskin and Sholl,[23] and Walton *et al.*[24] in IRMOF-1 and by Yang and Zhong[25–27] in both Cu-BTC and IRMOF-1 structures. Liu *et al.*[28] used experimental and theoretical methods to study the adsorption behavior of N_2 in Cu-BTC and Wang *et al.*[29] investigated the sorption properties of Cu-BTC for N_2, CO_2, methane, ethane and CO_2–CH_4 mixtures by a series of experimental methods. Zhou *et al.*[30] measured adsorption isotherms for CH_4 in IRMOF-1 over a large temperature and pressure range, and Millward and Yaghi[31] compared the volumetric CO_2 capacity for a variety of MOFs. In this work we go one step further by analyzing the molecular siting during the adsorption of the main components of natural gas and their mixtures. We use molecular simulations to obtain information about the performance of two highly porous MOFs, Cu-BTC and IRMOF-1, in the natural gas separation process. Cu-BTC (BTC: benzene-1,3,5-tricarboxylate) has garnered a good deal of attention since it was first reported by Chui *et al.*[32] in 1999. Its framework is a metal coordination polymer based on copper as the metal centre and benzene-1,3,5-tricarboxylates as the linker molecule. It is formed by primary building blocks connected to form a face-centered cubic crystal framework, and secondary building blocks forming octahedron-shaped pockets accessible for small molecules through small windows. IRMOF-1 belongs to the family of isoreticular metal–organic frameworks (IRMOFs) and was first synthesized by Yaghi and co-workers.[12,13] IRMOF-1 structure consists of a cubic array of $Zn_4O(CO_2)_6$ units connected by phenylene links. The linkage of the Zn_4O complexes is forced to alternate between linkers pointing outwards and inwards, resulting in a structure with two alternating type of cavities. The small cavities are about 10.9 Å and larger cavities are about 14.4 Å diameter.[13]

This work analyzes the storage capacity and adsorption behavior of CH_4, C_2H_6, N_2, CO_2, C_3H_8 and the separation of their mixtures in Cu-BTC and IRMOF-1. We focus not only

Department of Physical, Chemical, and Natural Systems, University Pablo de Olavide, Ctra. Utrera km. 1., 41013 Seville, Spain. E-mail: scalero@upo.es; Fax: +34 954 349814; Tel: +34 954 977594

† Electronic supplementary information (ESI) available: Complete set of parameters and charges for adsorbates and adsorbents; additional Figures 1s–9s; center-of-mass distribution movies 1–2; movie 3 showing molecular siting; and Tables summarizing the occupancies of the sites. See DOI: 10.1039/b807470d

on the adsorption capacities and selectivities but also on the preferential adsorption sites of the components as a function of pressure. In section II we describe the simulation methods and the models used for the MOFs and the adsorbates. The obtained adsorption isotherms, molecular siting, and occupancies for pure components and mixtures are presented in section III, followed by some concluding remarks in section IV.

II. Simulation methods and models

Adsorption isotherms were calculated using grand canonical Monte Carlo (GCMC) simulations, where the chemical potential, the temperature and the volume are kept fixed. The fugacity, related directly to the imposed chemical potential,[33] is obtained from the value of pressure using the Peng–Robinson equation of state. We used at least 10^7 MC cycles that consist of translation, rotation, regrowth in random positions and change of identity for mixtures.[34] For comparison with experimental isotherms, absolute adsorption was converted to excess adsorption.[18,35]

Atomic interactions were described by Lennard-Jones and Coulomb potentials computed with the Ewald summation technique, using a relative precision of 10^{-6}. The Lennard-Jones potential is cut and shifted with a cutoff distance of 12 Å. The parameters for methane, ethane, and propane were taken from the united atom TraPPE model[36] in which the CH_x beads are considered as single, chargeless interaction centers. The beads are connected using a harmonic bond-potential $U = 0.5\,k\,(r - r_0)^2$ with $k/k_B = 96\,500$ K and $r_0 = 1.54$ Å, and a harmonic bend potential $U = 0.5\,k\,(\theta - \theta_0)^2$ with $k/k_B = 62\,500$ K and $\theta_0 = 114^\circ$. CO_2 and N_2 were considered as small rigid molecules, using the model proposed by Harris *et al.*[37] for CO_2 and the model proposed by Murthy *et al.*[38] for N_2. The partial charges of N_2 and CO_2 are distributed along each molecule to reproduce the experimental quadrupole moment. These models and potentials have been successfully employed to describe the adsorption in zeolites.[39–42]

Cu-BTC and IRMOF-1 frameworks are considered rigid with Lennard-Jones parameters taken from the DREIDING[43] force field except those for Cu, which were taken from the UFF[44] force field. Lorentz–Berthelot mixing rules were used to calculate mixed Lennard-Jones parameters and the atomic charges for the MOFs were taken from Frost *et al.* and Dubbeldam *et al.*[45] One unit cell of the IRMOF-1 ($a = b = c = 25.832$ Å) and one unit cell of Cu-BTC ($a = b = c = 26.343$ Å) were used during the simulations. We obtained a helium void fraction of 0.82 for IRMOF-1 and 0.76 for Cu-BTC. The crystal structure of Chui *et al.* includes axial oxygen atoms weakly bonded to the Cu atoms, which correspond to water ligands. Our simulations have been performed on the dry Cu-BTC with these oxygen atoms removed. The complete set of parameters and charges used in this work for adsorbates and adsorbents is listed in the ESI (Table 1s).†

The method used for the analysis of preferential adsorption sites in MOFs is similar to that used on the locations and occupancies of ions in zeolites.[46,47] We have defined eight individual adsorption sites for IRMOF-1 and four for Cu-BTC, based on previous works that studied the adsorption sites of argon and nitrogen in IRMOF-1[48,49] and hydrogen in Cu-BTC.[28] The IRMOF-1 unit cell contains 8 Zn_4O tetrahedral clusters and 24 linker molecules, defining 4 small cavities and 4 large cavities (see Fig. 1s of the ESI†). Five of the sites defined for IRMOF-1 are close to the Zn_4O cluster and the linker molecules (sites I to V) and the other three form a second layer in the pores (sites VI to VIII). Sites I and II are located in the large and small cages, respectively. Site III is located in the region that separates both types of cages. Sites IV and V are close to the linker molecules, above and beneath the center of the phenyl ring (site IV) and on the edges of it (site V). Sites VI and VII forming a layer above site IV, and site VIII located at the center of the small cage, above site II and surrounded by site V.

Cu-BTC is composed using benzene-1,3,5-tricarboxylate (BTC) ligands to coordinate copper ions, forming big cavities and small octahedral cages (see Fig. 2s of the ESI†). We have defined four adsorption sites on this structure; the sites labeled I, II, and III described by Liu *et al.* as preferential adsorption sites for H_2 and one additional site that we labeled I′. Sites I and I′ are located at the big central cavities, in the center (site I′) or close to the Cu^{2+} atoms (site I), and sites II and III are located at the center and at the windows of the small octahedral cages, respectively. More details about the structure and adsorption sites for IRMOF-1 and Cu-BTC can be found in the ESI† (Fig. 3s, 4s, and 5s).

III. Results

The adsorption isotherms and preferential adsorption sites in Cu-BTC and IRMOF-1 were obtained at 298 K for: (1) pure component methane, ethane, propane, nitrogen and carbon dioxide; (2) 50 : 50 and 90 : 10 CH_4–CO_2 binary mixtures; (3) 90 : 10 N_2–CO_2 binary mixtures; and (4) 95 : 2 : 1.5 : 1 : 0.5 five component mixtures of methane, ethane, nitrogen, carbon dioxide and propane.

Adsorption of pure components

Simulated and available experimentally measured adsorption isotherms of pure methane, ethane and propane in Cu-BTC and IRMOF-1 as a function of pressure are shown in Fig. 1a and b, respectively. The simulated isotherms are in good agreement with previous simulation results and experimental data.[22,26,27,29,30,35,45,50–52] The adsorption of the hydrocarbons increases with the number of carbon atoms in both structures for the complete pressure range under study. This is due to a combination of energetic effects and size entropic effects.[53] At much higher pressures near saturation (not shown here) methane would absorb more as a consequence of shape entropic effect[53] (methane fits better than ethane and propane into the partially occupied cavities). Adsorption isotherms of CO_2 and N_2 are shown in Fig. 2a (Cu-BTC), and Fig. 2b (IRMOF-1). The simulation results obtained for IRMOF-1 are in very good agreement with previous experimental values.[29,31] The agreement is also good for Cu-BTC at low pressures[22,26,31,45,52,54] though deviations are observed at higher pressures, where simulation data overestimates measured values for CO_2. Those deviations can be attributed to the force

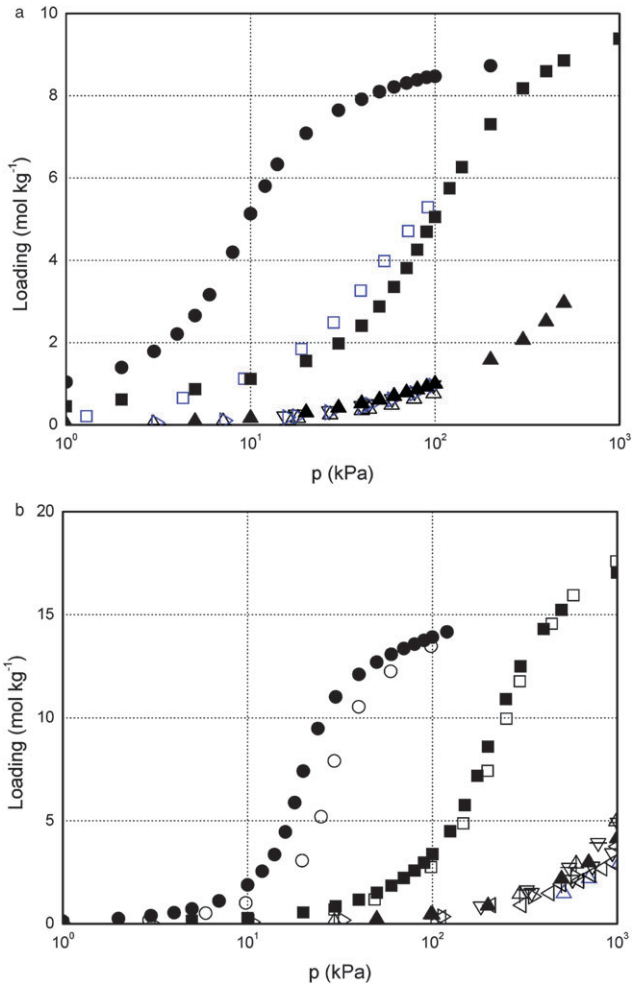

Fig. 1 Adsorption isotherms of pure methane (triangles), ethane (squares), and propane (circles) in (a) Cu-BTC and in (b) IRMOF-1 at 298 K. Our simulated isotherms (full symbols) are compared with previous experimental data[29,30] (blue open symbols) and simulation data[22,26,27,35,45,50–52] (black open symbols).

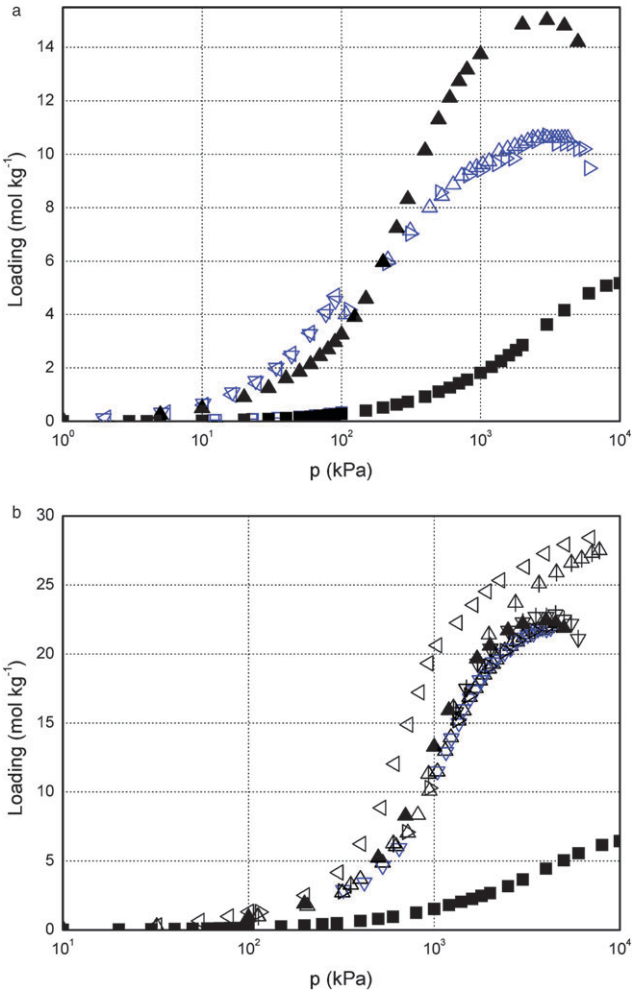

Fig. 2 Adsorption isotherms of pure CO_2 (triangles) and N_2 (squares) in (a) Cu-BTC and in (b) IRMOF-1 at 298 K. Our simulated isotherms (full symbols) are compared with previous experimental data[29,31] (blue open symbols) and simulation data (black open symbols).

field accuracy and also to the fact that our framework is a rigid and perfect material, whereas experimental samples are flexible and they generally contain water and organic residues after synthesis, leading to a decrease in the storage capacity. The partially charged CO_2 has a stronger interaction with the framework than N_2 and, therefore, higher adsorption. For the same reason, the extent of CO_2 adsorption is larger than that of methane in both MOFs over the entire pressure range under study, in which saturation is not reached. Direct comparison of the obtained adsorption isotherms for hydrocarbons and for N_2 and CO_2 for both structures proves that Cu-BTC is the best adsorbent at the lower pressures, while IRMOF-1—with a larger pore volume and therefore larger storage capacity—is the best adsorbent at the higher pressures (see Fig. 6sa and 6sb of the ESI†). This can be attributed to entropic effects, since the molecular packing is more efficient in the small octahedral cages of Cu-BTC—preferential adsorption sites at low pressures—than in the big cavities of IRMOF-1. The ESI† contains movies taken directly from our simulations that illustrate the molecular siting as a function of pressure (Movies 1 and 2).

Snapshots showing the adsorption behavior of carbon dioxide and methane at increasing pressure are shown in Fig. 3a and b.

The adsorption behavior of carbon dioxide and methane as a function of pressure in Cu-BTC is depicted in Fig. 3a and b. At low pressures methane preferentially adsorbs in the small octahedral cages of Cu-BTC (site II), while CO_2 not only adsorbs in the cages but also in the windows (site III). The adsorption of N_2 in the big cages (site I′) is as important as in the octahedral cages, and the windows are also occupied (site III) but in a lower extent. Site II is also preferential adsorption site for longer alkanes at low pressures and the increase in the number of carbon atoms in the chain progressively reduces the adsorption on site III, being almost zero for propane. At higher pressures and once the octahedral cages are partially filled, the molecules adsorb more in the big cage (site I′) and in the windows (site III). Site I, defined by Liu *et al.* as a preferential adsorption position for hydrogen[55] remains empty for all adsorbates over the entire range of pressures.

A similar study was done for IRMOF-1, identifying the large cages (site I) and the region that separates large and

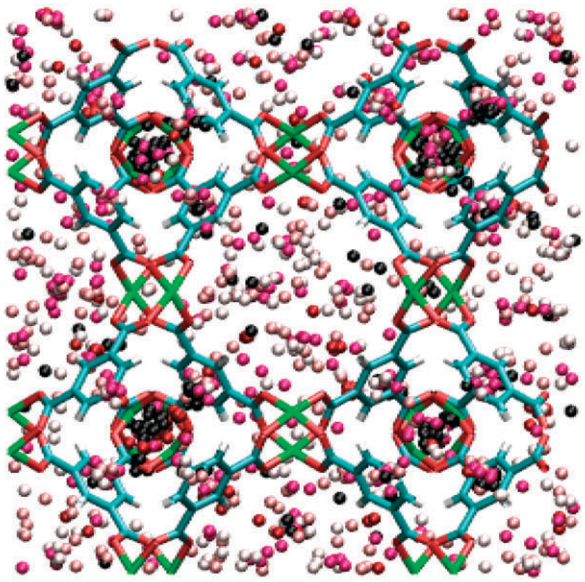

(a)

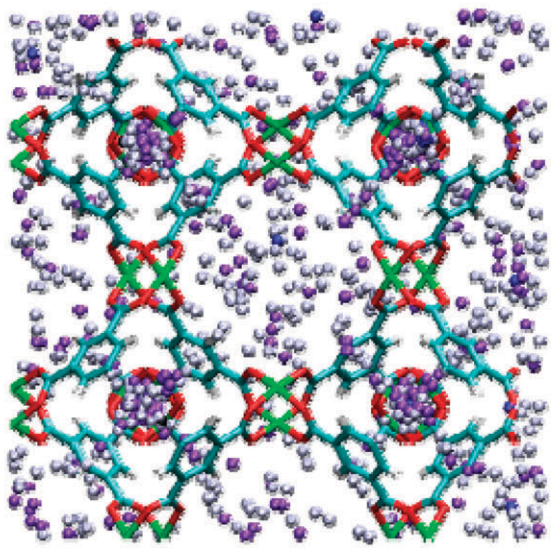

(b)

Fig. 3 Center-of-mass distributions of (a) carbon dioxide and (b) methane molecules adsorbed in Cu-BTC at 298 K for 2 kPa, 20 kPa, 200 kPa, 1000 kPa and 5000 kPa. The center of mass changes from darker to lighter color with increasing pressure. Simulations were performed using one (2 kPa), two (20 kPa), and four million (200 to 5000 kPa) MC steps. The snapshots are taken every 5000 steps for 2 kPa, 10 000 steps for 20 kPa, and 20 000 steps for the three higher pressures.

small cages (site III) as preferential adsorption sites for pure component adsorption. Site III shows the highest occupation, followed by site I. Site II (small cages) was found almost empty. Most of the adsorbed molecules close to the linkers are found above and beneath the center of the phenyl ring (site IV) and only a few molecules are on the edges of the linkers (site V). Two out of the three additional sites described by Rowsel *et al.* for argon molecules[48] show very little adsorption in all cases. Those are the sites labeled as VI and VII that form a layer above the phenyl ring. The third additional site (site VIII) is almost empty at low pressures but a significant increase of adsorption is observed at higher pressures. Tables summarizing the occupancies of the sites by all pure components at 298 K in Cu-BTC and IRMOF-1 can be found in the ESI† (Tables 2s and 3s).

Adsorption of CH_4 and CO_2 binary mixtures

Fig. 4 shows the computed adsorption selectivity for CO_2 relative to CH_4 defined as $(x_{CO_2}/y_{CO_2})/(x_{CH_4}/y_{CH_4})$, where x_{CO_2} and x_{CH_4} are the molar fractions in the adsorbed phase and y_{CO_2} and y_{CH_4} are the molar fractions in the bulk phase. Selectivities were computed for the 50 : 50 and for the 10 : 90 CO_2–CH_4 mixtures. The selectivity in Cu-BTC is the highest among the two adsorbents. CO_2 preferentially adsorbs in both MOFs due to the stronger interactions between the CO_2 molecules and the surfaces. Previous simulation data[22,23,26]—only available for the 50 : 50 equimolar mixture—were added for comparison, showing very good agreement for IRMOF-1. The selectivity for Cu-BTC obtained by simulations show similar trends than the experimentally-obtained value, but the deviation is larger than for IRMOF-1. The force field used in this work is less accurate for Cu-BTC than for IRMOF-1 and a very small deviation in the number of adsorbed molecules may result in a larger deviation in selectivity. The selectivity in Cu-BTC is the highest among the two adsorbents despite the deviations, suggesting that this structure is a potentially good candidate to separate CO_2 and CH_4.

The analysis of adsorption sites for the previous mixtures in Cu-BTC shows that at low pressures methane preferentially adsorbs in the octahedral cages displacing an important fraction of CO_2 molecules to the windows. At higher pressures and once the octahedral cages are full, site I′ becomes the preferential adsorption site. The equilibrium snapshots are depicted in Fig. 5. The siting of methane and CO_2 molecules during

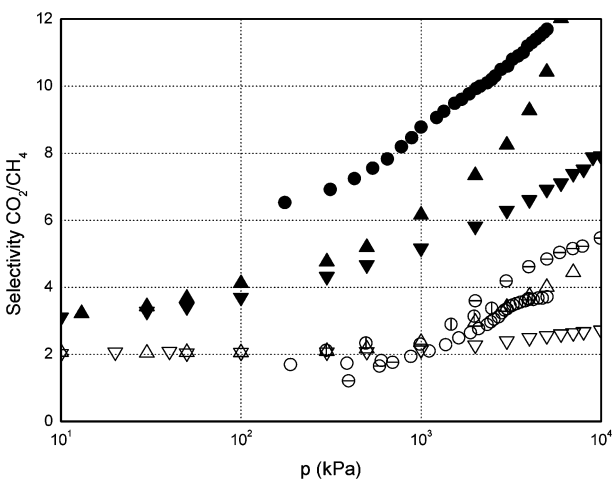

Fig. 4 Selectivity for CO_2 from the equimolar and the 10 : 90 mixture of CO_2 and methane in Cu-BTC (full symbols) and IRMOF-1 (open symbols) at 298 K. Our simulation results (up triangles for the equimolar and down triangles for the 10 : 90 mixture) are compared with previous simulation data[22,23,26] (different style of circles) available only for the equimolar mixtures.

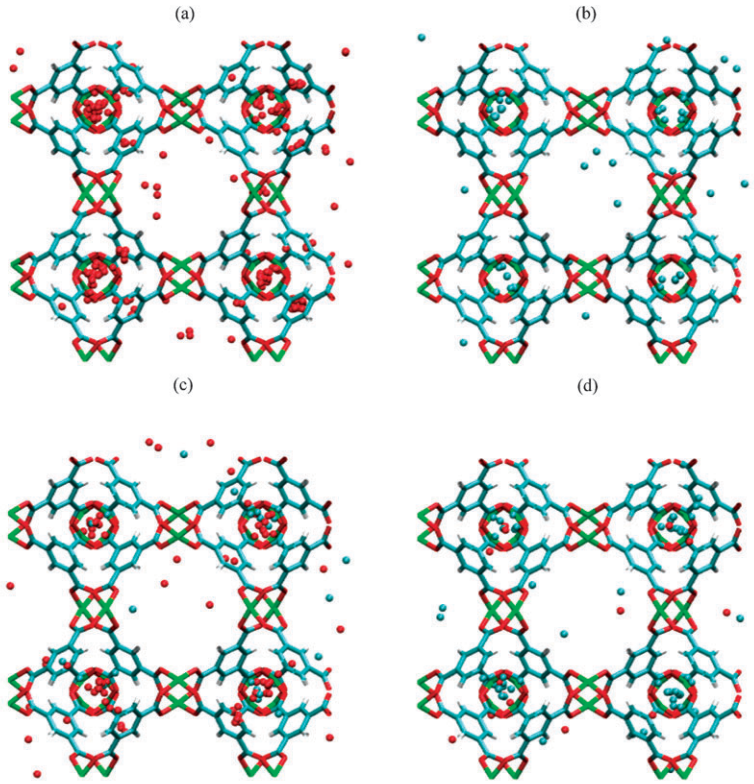

Fig. 5 Adsorption of molecules in Cu-BTC at 2 kPa and 298 K. Snapshots were taken every 5000 steps in a simulation of one million MC steps, and all the molecules in them were plotted. Only the center of mass of the molecules are drawn, CO_2 in red and methane in blue. (a) Pure CO_2, (b) pure methane, (c) 50 : 50 mixture CO_2–methane, and (d) 10 : 90 mixture CO_2–methane.

adsorption of the binary mixture in IRMOF-1 shows the same trend as the pure components, the large cages and the region that separates the large and the small cages being the preferential adsorption sites. The ESI† contains movies taken directly from our simulations that illustrate the molecular siting as a function of pressure, and Tables summarizing the occupancies of the sites by the components of the mixtures at 298 K. (Tables 4s to 7s and Movie 3).

Adsorption of CO_2 and N_2 binary mixtures

Fig. 6 shows simulated adsorption selectivities for CO_2 relative to N_2 for the 10 : 90 CO_2–N_2 binary mixtures in both structures. The complete excess adsorption isotherms can be found in the ESI† (Fig. 7s). Our results confirm a very strong preferential adsorption of CO_2 over N_2. This selectivity is much higher in Cu-BTC than in IRMOF-1 but the general trend is similar in the two materials and remains constant with pressure for the range that spans from 1 to 10^2 kPa. The selectivity for carbon dioxide from the binary mixture increases at higher pressures, and this increase is sharper in Cu-BTC than in IRMOF-1. This can be attributed to the differences in structure. The pores of Cu-BTC are smaller than those of IRMOF-1, leading to stronger confinement effects for CO_2 and favoring its packing.

The analysis of the adsorption sites in Cu-BTC for this mixture shows competition for the octahedral cages. At low pressures, the order of preferential adsorption for carbon dioxide is site II > site III > site I′, whereas for nitrogen is site I′ > site II > site III. At the highest pressures the octahedral cages and the windows are already full increasing then the adsorption in the big cages (site I′). The siting of CO_2 and N_2 in IRMOF-1 is similar to that for the pure components. The molecules preferentially adsorb in the large accessible cages and in the region that separates both types of cages, and most of the molecules adsorbed close to the linkers are located above and beneath the center of the phenyl ring (see Tables 8s and 9s of the ESI†).

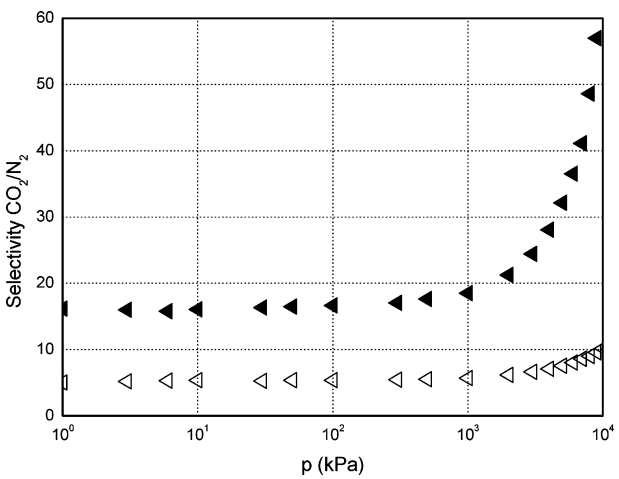

Fig. 6 Selectivity for CO_2 from the 10 : 90 binary mixture of CO_2 and N_2 in Cu-BTC (full symbols) and IRMOF-1 (open symbols) at 298 K.

Adsorption of the five-component mixture

Fig. 7 shows the adsorption of a five-component mixture of methane, ethane, nitrogen, carbon dioxide, and propane in Cu-BTC (Fig. 7a) and IRMOF-1 (Fig. 7b) at the bulk partial fugacity ratio of 95 : 2.0 : 1.5 : 1.0 : 0.5. The isotherms show similar adsorption for all components but methane in both MOFs. At high pressures the amount of methane adsorbed in IRMOF-1 is larger than in Cu-BTC since the cavities of the former are bigger than those of the latter. The selectivity between carbon dioxide and methane is similar to that of the corresponding binary systems as shown in Fig. 8. Again the carbon dioxide adsorption selectivity in Cu-BTC is much larger than in IRMOF-1, with a clearer increase with increasing pressure. This can be attributed to the combination of two effects: first, the electrostatic interactions between the carbon dioxide and the framework—that enhance CO_2 adsorption in both structures; and second, the strong confinement effects in the octahedral cages of Cu-BTC—that enhance the selectivity of carbon dioxide in this structure.

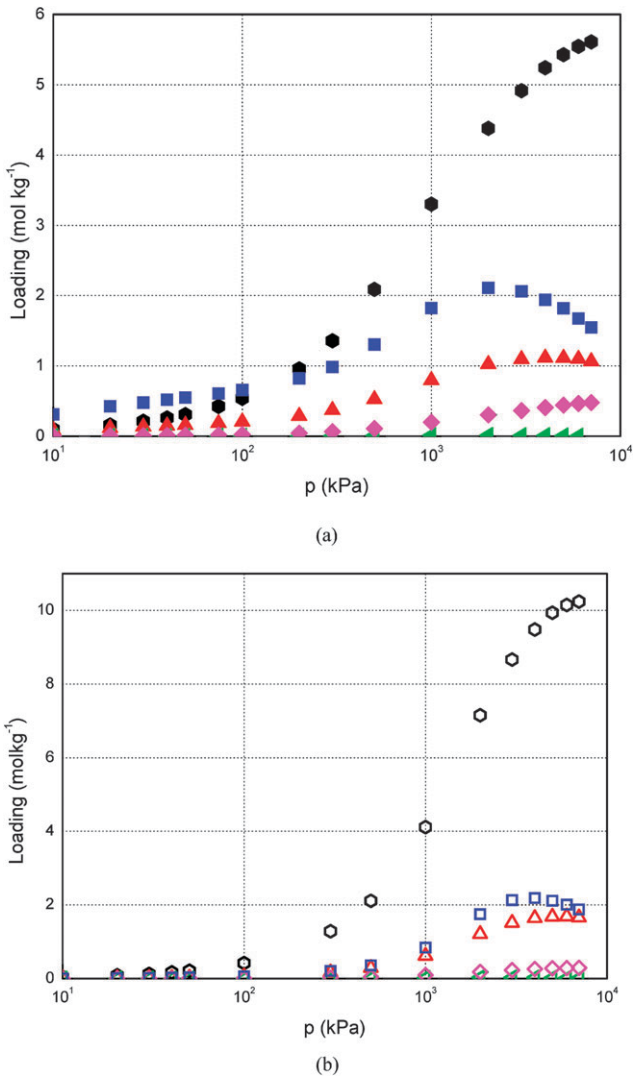

Fig. 7 Excess adsorption for the 95 : 2.0 : 1.5 : 1.0 : 0.5 mixture of methane (circles), ethane (triangles), N_2 (left triangles), CO_2 (rhombus) and propane (squares) in (a) Cu-BTC and (b) IRMOF-1 at 298 K.

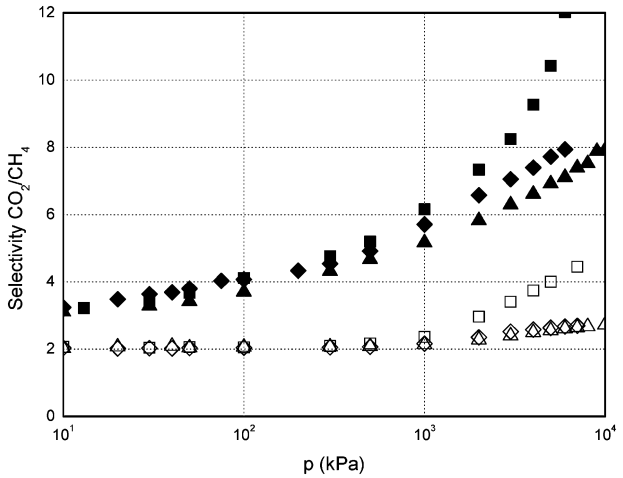

Fig. 8 Selectivity CO_2–CH_4 from the equimolar binary mixture (up triangles) and the 10 : 90 binary mixture (down triangles) compared with the selectivity CO_2–CH_4 from the five components mixture (squares) in Cu-BTC (full symbols) and IRMOF-1 (open symbols) at 298 K. The CO_2–CH_4 composition ratio in the bulk for the five components mixture is 1 : 95.

Analysis of the adsorption sites in Cu-BTC and IRMOF-1 for this mixture was further performed and shows that the molecular siting for the mixture is similar to that observed for the pure components in both structures. The detailed distribution is listed in Tables 10s and 11s of the ESI.†

IV. Conclusions

We have investigated the adsorption behavior of the main components of natural gas in Cu-BTC and IRMOF-1 using Monte Carlo simulations. We computed adsorption isotherms at 298 K for pure components and mixtures, and analyzed the preferential adsorption sites on these two MOFs. The detailed study of the siting of the molecules in both structures provided an explanation for the high adsorption capacity of IRMOF-1 and for the high adsorption selectivity towards carbon dioxide of Cu-BTC. On the basis of our observations, IRMOF-1 seems a good material for the storage of the different components of natural gas, whereas Cu-BTC could be a promising material for their separation.

Acknowledgements

This work is supported by the Spanish "Ministerio de Educación y Ciencia (MEC)" (CTQ2007-63229), Junta de Andalucía (Excellence Project 2008–2010), and by the resources, technical expertise and assistance provided by BSC-CNS. The authors wish to thank D. Dubbeldam and R. Krishna for useful discussions and Houston Frost and Randall Q. Snurr for making the Cu-BTC charges available to us before publication. E. García-Pérez, thanks the MEC for her predoctoral fellowship.

References

1 G. P. Brasseur, J. J. Orlando and G. S. Tyndall, *Atmospheric Chemistry and Global Change*, Oxford University Press USA, 1999.
2 R. J. Heinsohn and R. L. Kabel, *Sources and Control of Air Pollution*, Prentice Hall, 1999.
3 D. N. Dybtsev, H. Chun, S. H. Yoon, D. Kim and K. Kim, *J. Am. Chem. Soc.*, 2004, **126**, 32–33.
4 A. J. Fletcher, E. J. Cussen, D. Bradshaw, M. J. Rosseinsky and K. M. Thomas, *J. Am. Chem. Soc.*, 2004, **126**, 9750–9759.
5 O. Ohmori, M. Kawano and M. Fujita, *Angew. Chem., Int. Ed.*, 2005, **44**, 1962–1964.
6 L. Pan, K. M. Adams, H. E. Hernandez, X. T. Wang, C. Zheng, Y. Hattori and K. Kaneko, *J. Am. Chem. Soc.*, 2003, **125**, 3062–3067.
7 J. L. C. Rowsell and O. M. Yaghi, *Microporous Mesoporous Mater.*, 2004, **73**, 3–14.
8 R. Q. Snurr, J. T. Hupp and S. T. Nguyen, *AIChE J.*, 2004, **50**, 1090–1095.
9 O. M. Yaghi, M. O'Keeffe, N. W. Ockwig, H. K. Chae, M. Eddaoudi and J. Kim, *Nature*, 2003, **423**, 705–714.
10 A. J. Fletcher, K. M. Thomas and M. J. Rosseinsky, *J. Solid State Chem.*, 2005, **178**, 2491–2510.
11 J. L. C. Rowsell and O. M. Yaghi, *Angew. Chem., Int. Ed.*, 2005, **44**, 4670–4679.
12 M. Eddaoudi, J. Kim, N. Rosi, D. Vodak, J. Wachter, M. O'Keeffe and O. M. Yaghi, *Science*, 2002, **295**, 469–472.
13 H. Li, M. Eddaoudi, M. O'Keeffe and O. M. Yaghi, *Nature*, 1999, **402**, 276–279.
14 M. Eddaoudi, H. L. Li and O. M. Yaghi, *J. Am. Chem. Soc.*, 2000, **122**, 1391–1397.
15 M. Eddaoudi, D. B. Moler, H. L. Li, B. L. Chen, T. M. Reineke, M. O'Keeffe and O. M. Yaghi, *Acc. Chem. Res.*, 2001, **34**, 319–330.
16 B. L. Chen, M. Eddaoudi, S. T. Hyde, M. O'Keeffe and O. M. Yaghi, *Science*, 2001, **291**, 1021–1023.
17 A. G. Wong-Foy, A. J. Matzger and O. M. Yaghi, *J. Am. Chem. Soc.*, 2006, **128**, 3494–3495.
18 T. Duren, L. Sarkisov, O. M. Yaghi and R. Q. Snurr, *Langmuir*, 2004, **20**, 2683–2689.
19 L. Pan, H. M. Liu, X. G. Lei, X. Y. Huang, D. H. Olson, N. J. Turro and J. Li, *Angew. Chem., Int. Ed.*, 2003, **42**, 542.
20 J. Y. Lee, L. Pan, S. R. Kelly, J. Jagiello, T. J. Emge and J. Li, *Adv. Mater.*, 2005, **17**, 2703.
21 S. Wang, Q. Y. Yang and C. L. Zhong, *Sep. Purif. Technol.*, 2008, 30–35.
22 R. Babarao, Z. Q. Hu, J. W. Jiang, S. Chempath and S. I. Sandler, *Langmuir*, 2007, **23**, 659–666.
23 S. Keskin and D. S. Sholl, *J. Phys. Chem. C*, 2007, **111**, 14055–14059.
24 K. S. Walton, A. R. Millward, D. Dubbeldam, H. Frost, J. J. Low, O. M. Yaghi and R. Q. Snurr, *J. Am. Chem. Soc.*, 2008, **130**, 406.
25 Q. Y. Yang, C. Y. Xue, C. L. Zhong and J. F. Chen, *AIChE J.*, 2007, **53**, 2832–2840.
26 Q. Y. Yang and C. L. Zhong, *J. Phys. Chem. B*, 2006, **110**, 17776–17783.
27 Q. Y. Yang and C. L. Zhong, *ChemPhysChem*, 2006, **7**, 1417–1421.
28 J. C. Liu, J. T. Culp, S. Natesakhawat, B. C. Bockrath, B. Zande, S. G. Sankar, G. Garberoglio and J. K. Johnson, *J. Phys. Chem. C*, 2007, **111**, 9305–9313.
29 Q. M. Wang, D. M. Shen, M. Bulow, M. L. Lau, S. G. Deng, F. R. Fitch, N. O. Lemcoff and J. Semanscin, *Microporous Mesoporous Mater.*, 2002, **55**, 217–230.
30 W. Zhou, H. Wu, M. R. Hartman and T. Yildirim, *J. Phys. Chem. C*, 2007, **111**, 16131–16137.
31 A. R. Millward and O. M. Yaghi, *J. Am. Chem. Soc.*, 2005, **127**, 17998–17999.
32 S. S. Y. Chui, S. M. F. Lo, J. P. H. Charmant, A. G. Orpen and I. D. Williams, *Science*, 1999, **283**, 1148–1150.
33 E. Beerdsen, B. Smit and S. Calero, *J. Phys. Chem. B*, 2002, **106**, 10659–10667.
34 R. Krishna, B. Smit and S. Calero, *Chem. Soc. Rev.*, 2002, **31**, 185–194.
35 T. Duren and R. Q. Snurr, *J. Phys. Chem. B*, 2004, **108**, 15703–15708.
36 M. G. Martin and J. I. Siepmann, *J. Phys. Chem. B*, 1998, **102**, 2569–2577.
37 J. G. Harris and K. H. Yung, *J. Phys. Chem.*, 1995, **99**, 12021–12024.
38 C. S. Murthy, K. Singer, M. L. Klein and I. R. McDonald, *Mol. Phys.*, 1980, **41**, 1387–1399.
39 E. Garcia-Perez, J. B. Parra, C. O. Ania, A. Garcia-Sanchez, J. M. Van Baten, R. Krishna, D. Dubbeldam and S. Calero, *Adsorption*, 2007, **13**, 469–476.
40 E. García-Pérez, J. B. Parra, C. O. Ania, J. M. van Baten, R. Krishna and S. Calero, *Appl. Surf. Sci.*, 2006.
41 D. Dubbeldam, S. Calero, T. J. H. Vlugt, R. Krishna, T. L. M. Maesen, E. Beerdsen and B. Smit, *Phys. Rev. Lett.*, 2004, 93.
42 D. Dubbeldam, S. Calero, T. J. H. Vlugt, R. Krishna, T. L. M. Maesen and B. Smit, *J. Phys. Chem. B*, 2004, **108**, 12301–12313.
43 S. L. Mayo, B. D. Olafson and W. A. Goddard, *J. Phys. Chem.*, 1990, **94**, 8897–8909.
44 A. K. Rappe, C. J. Casewit, K. S. Colwell, W. A. Goddard and W. M. Skiff, *J. Am. Chem. Soc.*, 1992, **114**, 10024–10035.
45 D. Dubbeldam, K. S. Walton, D. E. Ellis and R. Q. Snurr, *Angew. Chem., Int. Ed.*, 2007, **46**, 4496–4499.
46 S. Calero, D. Dubbeldam, R. Krishna, B. Smit, T. J. H. Vlugt, J. F. M. Denayer, J. A. Martens and T. L. M. Maesen, *J. Am. Chem. Soc.*, 2004, **126**, 11377–11386.
47 S. Calero, M. D. Lobato, E. Garcia-Perez, J. A. Mejias, S. Lago, T. J. H. Vlugt, T. L. M. Maesen, B. Smit and D. Dubbeldam, *J. Phys. Chem. B*, 2006, **110**, 5838–5841.
48 J. L. C. Rowsell, E. C. Spencer, J. Eckert, J. A. K. Howard and O. M. Yaghi, *Science*, 2005, **309**, 1350–1354.
49 D. Dubbeldam, H. Frost, K. S. Walton and R. Q. Snurr, *Fluid Phase Equilib.*, 2007, **261**, 152–161.
50 G. Garberoglio, A. I. Skoulidas and J. K. Johnson, *J. Phys. Chem. B*, 2005, **109**, 13094–13103.
51 J. W. Jiang and S. I. Sandler, *Langmuir*, 2006, **22**, 5702–5707.
52 A. I. Skoulidas and D. S. Sholl, *J. Phys. Chem. B*, 2005, **109**, 15760–15768.
53 R. Krishna, S. Calero and B. Smit, *Chem. Eng. J.*, 2002, **88**, 81–94.
54 Q. Y. Yang, C. L. Zhong and J. F. Chen, *J. Phys. Chem. C*, 2008, **112**, 1562–1569.
55 Y. Liu, C. M. Brown, D. A. Neumann, V. K. Peterson and C. J. Kepert, *J. Alloys Compd.*, 2007, **446**, 385–388.